submitted to *Geophys. J. Int.*

Real-time infrasonic monitoring of the eruption at a remote island volcano, Nishinoshima, Japan

Kiwamu Nishida and Mie Ichihara

Earthquake Research Institute, University of Tokyo, Yayoi 1, Bunkyo-ku, Tokyo 113-0032, Japan

SUMMARY

On November 20, 2013, a submarine eruption started close to Nishinoshima island, which lies ∼1000 km south of Tokyo. Real-time monitoring of the eruption is crucial for understanding the formation processes of the new volcano island and related disaster prevention. *In situ* monitoring, however, is difficult in practice because the closest inhabited island, Chichijima, is 130 km away from Nishinoshima. This study presents an infrasonic monitoring method that uses cross-correlating records at a pair of online stations on Chichijima. One is the horizontal ground velocity recorded at a permanent seismic station operated by the Japan Meteorological Agency (JMA). The seismic records were corrected for atmospheric pressure using an empirical ground response to infrasound. The other is the air pressure recorded at the JMA Meteorological Observatory. For each station, we divided the whole records into 3600-s segments. To suppress outliers, each segment was normalised by the envelope function. We then calculated cross-correlation functions between the pair of stations using the fast Fourier transform. They present clear successive arrivals of infrasound coming from Nishinoshima. We also conducted an offline tripartite-array observation using three low-frequency microphones with a station spacing of ∼50 m installed in May 2013. The array analysis supports the results obtained from the online stations. The typical root-mean-squared amplitude is on the order of 0.01 Pa, and the typical duration is several days. The amplitudes were primarily controlled by the effective sound velocity structure from Nishinoshima to Chichijima. The infrasonic observations together with the meteorological observation at Chichijima suggest that infrasonic

activity was not present in the first two weeks in January 2015. With the help of a more quantitative estimation of the meteorological effect, we could infer eruptive activity in real time.

Key words: infrasound, real-time monitoring, volcanic eruption

1 INTRODUCTION

Nishinoshima, an active volcanic island in the Izu-Ogasawara volcanic arc, lies ∼1000 km south of Tokyo. The volcano island is the summit of a huge volcano growing on the 3000-m-deep sea bottom. The last submarine eruptions began in April 1973, and a new volcano island appeared in August. In March 1974, the new island merged with the main island of Nishinoshima. Strombolian eruptions lasted until May 1974. From 1976 to 2000, sporadic seawater discolouration was observed around the island. On November 20, 2013, a new submarine eruption started at Nishinoshima. A new island emerged in November 2013, and it merged with the island of Nishinoshima on December 26, 2013. The area of the new island reached 2.3 km^2 in December 2014. It is still growing via lava flow and a central cone with a diameter of about 80 m is building up by Strombolian activity as of 2015.

Real-time monitoring of the eruption is crucial for evaluating the potential risk of eruption and understanding the formation process of the new volcano island. *In situ* monitoring is, however, difficult in practice, because the closest inhabited island, Chichijima, is 130 km away from Nishinoshima. Infrasonic observation is a useful tool for monitoring remote volcanos because infrasound can propagate long distances in the atmosphere (e.g., Fee et al. 2010; Le Pichon et al. 2005; Fee & Matoza 2013; Kamo et al. 1994). To detect a weak signal in a particular direction, multiple infrasonic stations in an array are needed (Ripepe 2002; Hedlin et al. 2012). However, only a small number of infrasonic arrays are being operated for volcano monitoring, although the number is now growing (Ripepe et al. 2010; Ulivieri et al. 2013; Ripepe et al. 2013) and many permanent seismic stations have been deployed at remote islands recently. Cross-correlation analysis using records between an infrasonic station and a seismic station is feasible for monitoring because seismic records are also sensitive to infrasound (Ichihara et al. 2012). Installation of another infrasonic sensor close to the seismic sensor (∼1 km) at a remote island is realistic for monitoring.

This study presents infrasonic monitoring of the remote volcano island Nishinoshima by cross-correlating the online seismic and infrasonic data from an accessible distant island, Chichijima. We will demonstrate the feasibility by a comparison with array analysis using three more offline infrasonic stations.

2 DATA

For monitoring, we used two online stations. One is a velocity meter with a natural frequency of 1 Hz located at a permanent seismic station operated by the Japan Meteorological Agency (JMA) (CHIJI3 shown in Figure 1(a)). Because the east–west component is more sensitive to infrasound in this observation, we used only that component. The seismic records were corrected for infrasonic waves by using an empirical ground response to infrasound as described in the next section. We installed a micro barometer (NanoBaro, Paroscientific Co.) at the JMA Meteorological Observatory (EV.CHI shown in Figure 1(a)), which is $\sim$1 km southeast of CHIJI3, in October 2014 with continuous data transmission to the Earthquake Research Institute of the University of Tokyo via a mobile-phone network. We also conducted an offline infrasonic observation using a tripartite array with a span of $\sim$50 m. Each element of the array was equipped with an infrasonic microphone (SI 102 or SI103, Hakusan Co.) and a data logger (LS8800, Hakusan Co.). All the records were sampled at 100 Hz. Together with the online data, we will discuss the potential for real-time monitoring of eruption activity at a remote volcano island from an accessible island.

The upper panel of Figure 1(b) shows a typical example of successive arrivals of impulses with peak amplitudes of about 1 Pa from Nishinoshima between 22:00 and 22:30 on November 23, 2014. The barograms and seismograms are bandpass-filtered from 2 to 8 Hz. The lower panel shows an enlargement of the impulses in a range of 20 s; one can see propagation with a phase velocity of $\sim$350 m/s. The amplitudes at CHIJI3, which is located on the ridge of Mt. Mikazuki (145 m), were slightly larger than those at other stations. The difference could be attributed to a shadow effect caused by the ridge. Such a high level of infrasonic activity typically lasted several days.

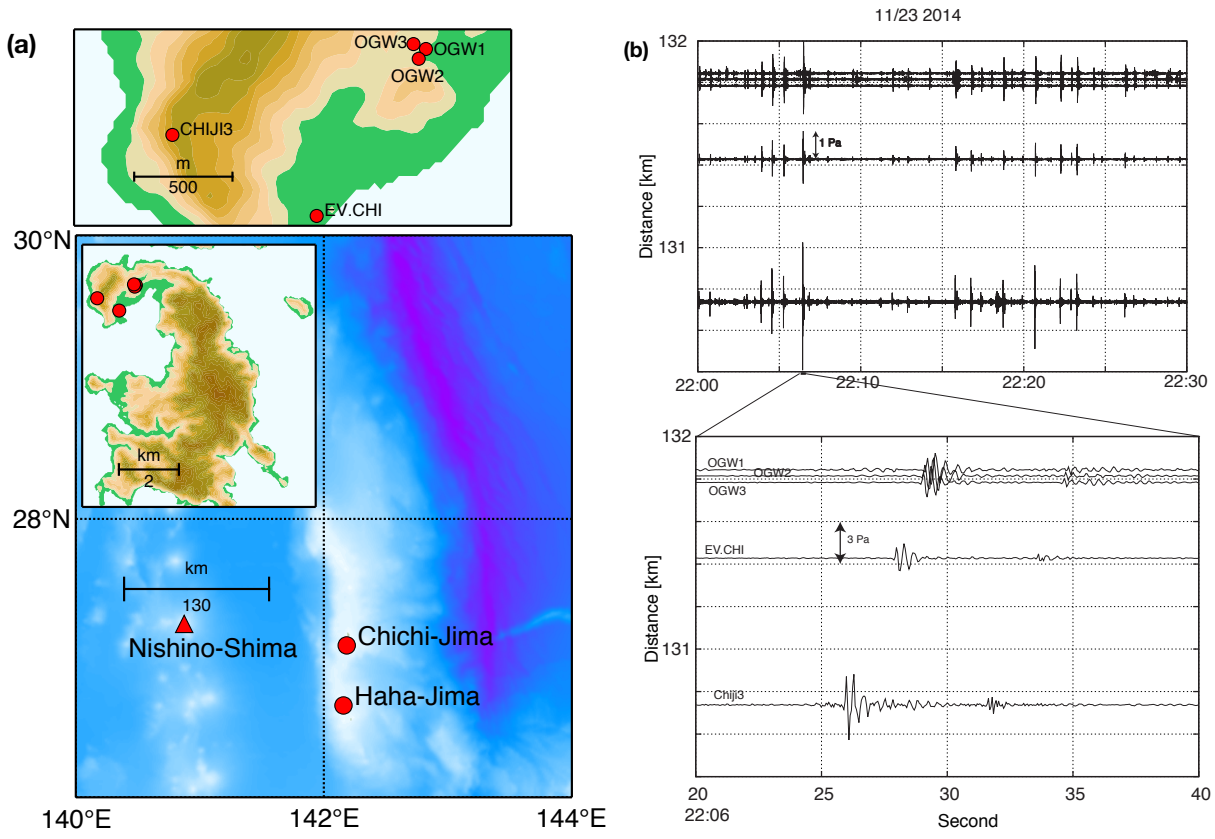

Figure 1. (a) Upper panel: Station distribution. Lower panel: Locations of Nishinoshima and Chichijima; the inset shows a magnified view around Chichijima. (b) A typical example of infrasonic records bandpass-filtered from 2 to 8 Hz on November 11, 2014. Ground velocity records at JMA station CHIJI3 were converted to atmospheric pressure using the empirical response function. The vertical axes show the distance from Nishinoshima.

3 SEISMIC RESPONSE TO INFRASOUND

To estimate the seismic response, we co-located a low-frequency microphone at CHIJI3 from February 21 to 24, 2015. Fortunately, we obtained large successive events from Nishinoshima. Using the infrasonic events from Nishinoshima, we estimated the response function. We simply corrected the response for the seismic records in this study.

The seismic response in the horizontal component at CHIJI3 was an order of magnitude larger than those of vertical ones. However, a simple model for a half infinite solid medium contact with a fluid medium (Ben-Menahem & Singh 2000; Ichihara et al. 2012) cannot explain this observation. A theoretical estimation suggests that the transfer function of infrasound to the vertical ground

velocity (H_{pw}) is a factor of 3 greater than that to the horizontal one (H_{pv}) for a Poisson medium because they are given by

$$H_{pw} = \frac{e^{-\pi/2} c_a}{2(\lambda+\mu)} \frac{\lambda+2\mu}{\mu},\ H_{pv} = \frac{c_a}{2(\lambda+\mu)}, \tag{1}$$

where c_a is the sound velocity and λ and μ are Lamé's constants (Ben-Menahem & Singh 2000):. The east–west component could be enhanced by a small-scale topography close to the observed station (cf. Fukao et al. 2010). When the infrasound meets a topographic feature whose scale is on the order of the wavelength, the net resultant force could be represented by a horizontal single force. The horizontal force could explain the observed dominance in the east–west component.

4 CROSS-CORRELATION ANALYSIS USING A PAIR OF ONLINE STATIONS

For real-time monitoring we conducted a cross-correlation analysis between a pressure record bandpass-filtered from 2 to 8 Hz at CHIJI3, u_0, and that at EV.CHI, u_1. Distortion of coherency caused by transient phenomena such as earthquakes recorded by the seismometer and glitches from packet loss complicate the analysis. To suppress them, the records were normalised by using the envelope functions ($\bar{u}_0$ and $\bar{u}_1$), which were estimated by using the absolute value of the corresponding analytical signal (Shen et al. 2012) as

$$\begin{aligned} \bar{u}_0(t) &= u_0(t)/\sqrt{u_0(t)^2 + \mathcal{H}(u_0(t))^2}, \\ \bar{u}_1(t) &= u_1(t)/\sqrt{u_1(t)^2 + \mathcal{H}(u_1(t))^2}, \end{aligned} \tag{2}$$

where $\mathcal{H}$ represents the Hilbert transform. Then we calculated a normalised cross-correlation function (nCCF) of the kth segments, $\bar{\phi}^k_{01}(\tau)$, between the pair with the envelope normalization as

$$\bar{\phi}^k_{01}(\tau) \equiv \frac{1}{\sqrt{\langle \bar{u}_0^2 \rangle \langle \bar{u}_1^2 \rangle}} \frac{1}{T} \int_{kT}^{(k+1)T} \bar{u}_0(t) \bar{u}_1(t+\tau) dt, \tag{3}$$

where T is the time length of the segment (1 hour), $\langle \bar{u}_i^2 \rangle$ are the mean-squared amplitudes, and τ represents the lag time. Figure 2(c) shows the resultant nCCFs with respect to time. We subtracted -1.87 s from the lag time for display, which is a rough estimation of the travel-time difference assuming the source at Nishinoshima. In Figure 2(c), the nCCF at each time segment is normalized by its maximum value in the displayed range of the reduced lag time ($-1 < \tau - 1.87 < 1$) for

the sake of better visualization of the signals. The maximum values, shown as the blue line in Figure 2(b), represent the coherency of the records. Larger values mean larger signal-to-noise ratios. These values show temporal variations with a typical duration of about 2–3 days.

In this study, the detection criterion for infrasound from Nishinoshima in a time segment is that the maximum of the nCCF is a factor of 10 greater than the median value in the segment. For the detected events, we estimated their root mean-squared amplitudes (RMS values) as follows. First we calculated un-normalised cross-correlation functions (CCFs) of the kth segments, $\phi_{01}^k(\tau)$, between the pair without the envelope normalization as

$$\phi_{01}^k(\tau) \equiv \frac{1}{T}\int_{kT}^{(k+1)T} \bar{u}_0(t)\bar{u}_1(t+\tau)dt, \tag{4}$$

Then, we selected the maximum values, which represent the power of the infrasound. Red dots in Figure 2(b) show the estimated RMS values of the detected events, which are the square root of the maximum CCF values.

5 ESTIMATIONS OF SLOWNESS VECTORS USING THE WHOLE ARRAY

The previous section described a method for real-time monitoring using a pair of stations. To interpret the results, we also used the data from the offline tripartite array (OGW1, OGW2, and OGW3 shown in Figure 1(a)). We estimated slowness vectors of the infrasonic events and the amplitudes (cf. Nishida et al. 2005) as follows, using all five stations (the three elements of the array and the two online stations).

First we measured the travel-time difference between each pair of stations by selecting the maximum of the nCCF. The detection criterion for an infrasonic event is that all the maxima are a factor of 5 greater than the corresponding median values. We estimated the slowness vector by minimising the squared differences of the travel-time differences assuming a plane wave. Figures 3(a) and (b) show the resultant incidental azimuths and horizontal apparent velocities, respectively. In this study, we neglected travel-time differences resulting from the vertical propagation of infrasound, because the estimated horizontal slowness shows almost horizontal propagation.

The RMS value of the detected event a_k at the kth segment was estimated by using the sum of

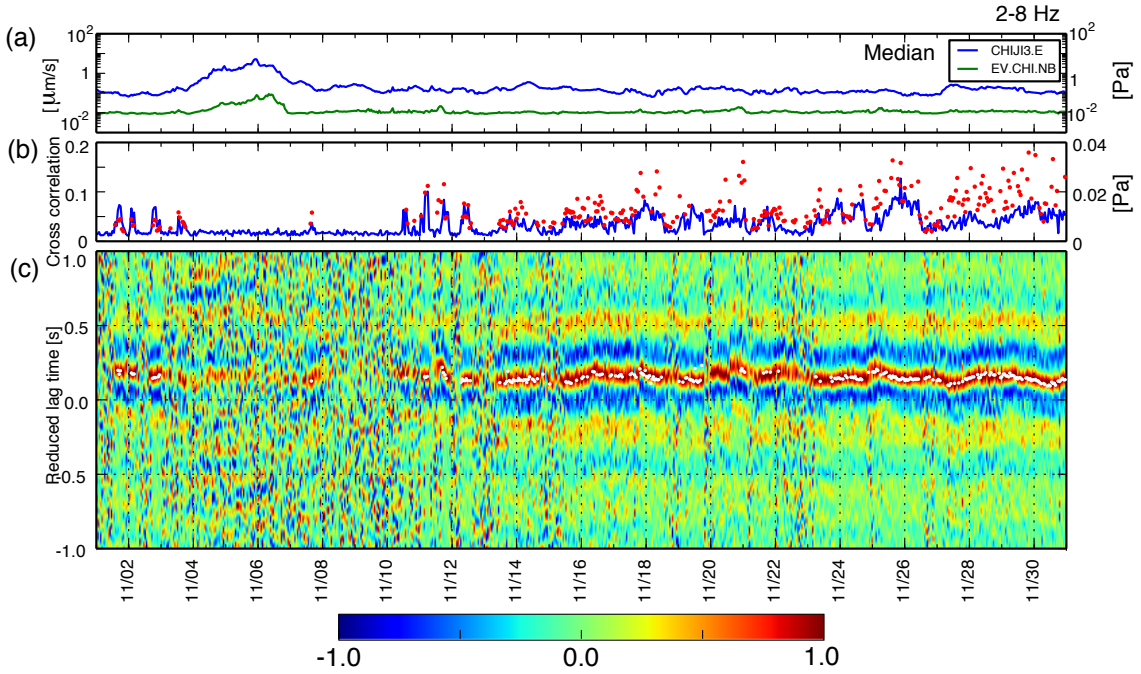

Figure 2. (a) RMS amplitudes of the seismometer at CHIJI3 and the micro barometer at EV.CHI calculated every hour from November 1 to 30, 2014. To suppress transients such as earthquakes and glitches, we applied a medium filter. (b) Maxima of the nCCFs shown by the blue line and mean squared amplitudes of the detected events shown by red dots. (c) The nCCFs between the pair of stations, normalised by the maximum values shown in Figure 2(b). We reduce a reference lag time of -1.87 s from the plot. We also show the lag time predicted by using the array analysis (white dots), which explains the peaks of the nCCF well.

CCFs at lag times between the individual pairs of the stations predicted by the estimated slowness vector of the infrasound as

$$a_k = \sqrt{\frac{1}{N}\sum_{i \neq j} \phi_{ij}^k (\delta t_i - \delta t_j)}, \tag{5}$$

where N is the number of the station pairs $(5 \times 4/2)$ and $(\delta t_i - \delta t_j)$ is the predicted travel-time difference between the ith and the jth stations obtained by using the estimated slowness vector. Here we note that we excluded autocorrelation functions ($i = j$), because they contain biases originating from local noise resulting from winds and instrumental noise. Black dots in Figure 3(c) show the resultant RMS amplitudes. The typical duration of the activity is several days. The typical time scales of the RMS temporal variations are similar to those of the incidental azimuths and the apparent velocity as shown in Figures 3(a) and (b). This similarity might be attributed to propagation effects owing to meteorological conditions between Nishinoshima and Chichijima,

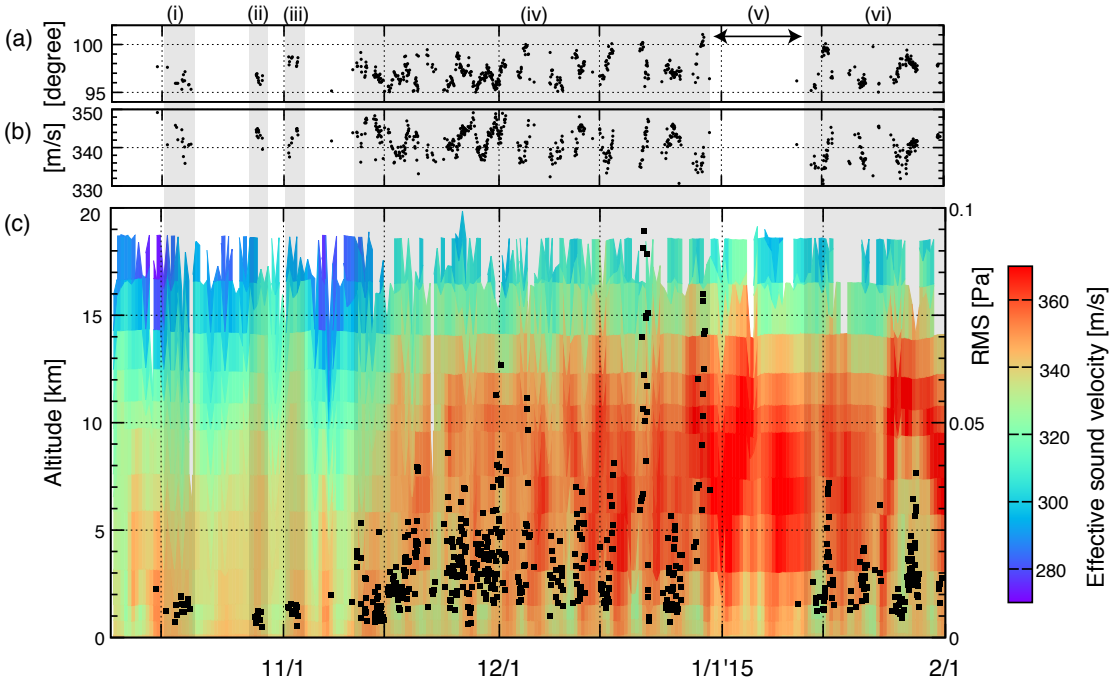

Figure 3. (a) Incidental azimuths of detected events. Shaded areas from (i) to (vI) show periods of the swarms. (b) Horizontal apparent velocities of the detected events. (c) RMS amplitudes of the events and the effective sound velocity for infrasound travelling from Nishinoshima to Chichijima calculated from the temperature and wind observed by a radiosonde at the JMA Meteorological Observatory. The red colour represents high velocity owing to high temperature and strong zonal winds.

as discussed in the next section. White dots in Figure 2(c) show the predicted lag times for the pair of online stations obtained by using the slowness vector. The resultant incidental azimuths and apparent velocities explain the observed travel-time differences between the pair of online stations.

6 DISCUSSION

6.1 Bias due to surf noise

At frequencies from 1 to 5 Hz, breaking ocean waves generate infrasound (Garcés 2003). This infrasound is excited persistently by random sources distributed on coastal areas. Although the ambient infrasound can be represented by a random wave field, it could also contribute to the nCCFs. Let us consider bias of the event detection caused by the ambient infrasound.

When the ambient infrasound is dominant, each nCCF shows two wave arrivals, which corre-

spond to wave propagation between the pair the stations as in seismic interferometry (Haney 2009). The two wave packets cause spurious incoming plane waves travelling along paths between pairs of stations. When we use only the tripartite array, the bias is more significant. The short interstation distance increases the contribution of the surf noise. This is because the amplitude of nCCFs originating from surf noise attenuates with the separation distance owing to geometrical spreading, whereas that of a plane wave from Nishinoshima does not depend on the propagation distance. When we use two more online stations, the longer separation distance of the stations suppresses false event detection resulting from the bias.

6.2 Comparison with atmospheric structures at Chichijima

The observed temporal variations of the slowness vectors could be explained by temporal changes of the effective sound speed (the adiabatic sound speed plus the wind speed in the direction of propagation from Nishinoshima to Chichijima) (Che et al. 2011; Le Pichon et al. 2005). Meteorological conditions could primarily control the observed infrasound. To discuss the meteorological effect qualitatively, we compared the results with the effective sound velocity for infrasound propagating from Nishinoshima to Chichijima. Here we assume a one-dimensional structure of sound velocity and zonal wind, which can be estimated from the temperature and wind observed by radiosonde at Chichijima. The observation is conducted twice a day (at 0:00 and 12:00 GMT) at the JMA Meteorological Observatory (EV.CHI shown in Figure 1). The estimated effective sound velocities are also shown in Figure 3(c).

From mid November 2014 to the end of January 2015, the figure shows a high-velocity "lid" at a height of $\sim$5 km. The infrasonic activity shown by black dots in Figure 3(c) correlates with the existence of the "lid", which is key for ducting infrasound propagation. The tropospherically ducted infrasound has considerable amplitude, because the ducting of the thin layer reduces geometrical spreading (Drob & Picone 2003). The one-dimensionality of the effective sound velocity structures is important for efficient ducting. The larger heat capacity of the ocean could also stabilise the effective sound velocity. Another factor for efficient propagation could be related to the roughness of the sea surface. When infrasound propagates above land, abrupt topographic changes

such as in the region of a volcano cause scattered reflection, which could disrupt the ducting (Lacanna et al. 2014). However, with propagation above a still ocean, the flat topography of the sea surface could stabilise the ducting.

The "lid" owes its origin to westerlies from winter to spring. The low-velocity channel below 5 km traps the infrasound, and it propagates effectively. In contrast, the lack of a high-velocity "lid" before mid November originates from the northern shift of westerlies (Ono & Irino 2004). Even before mid November, infrasonic amplitudes were detected sporadically, as shown by shaded areas from (i) to (iii) in Figure 3. These areas coincide with a weak "lid" caused by weaker zonal winds, as shown in Figure 3. The activity before mid November is so sensitive to tiny changes of zonal wind that the observations were controlled primarily by tiny changes of meteorological conditions.

After mid November, we can identify swarms of infrasonic events in periods (iv) and (vi) in Figure 3. The temporal variations could be related to the effective sound velocity. When the zonal winds were strong, even close to the surface, the low-velocity channel was weakened. In the absence of the low-velocity channel (identified as the lack of green colour all over from the surface to 15 km), fewer infrasonic events were detected. This coincidence suggests a possibility that the temporal variations of of the long-distance infrasonic propagations, that are controlled primarily by the wind condition, can be quantitatively evaluated by using the atmospheric data from the single weather station. Although the typical variation time scales of the azimuths and apparent velocity are also similar to that of the RMS amplitudes, their relation is complex.

The "lid" of the effective sound velocity in period (v) in Figure 3 suggests that several swarms of infrasonic activity should be observed intermittently at least. We note that the wind noise is not particularly strong in this period. The absence of such infrasonic activity in the period suggests that the eruptive activity was not present in the period. Any further discussion would require a new method for a quantitative estimation of the propagation effects owing to the apparent acoustic velocity structure between Nishinoshima and Chichijima.

7 CONCLUSIONS

For near-real-time monitoring of volcanic activity at the remote island of Nishinoshima, we analyzed online data from an infrasonic station and a seismic station at a distant inhabited island, Chichijima. Cross-correlation analyses were performed and the resultant nCCFs present clear successive arrivals of infrasound propagating from Nishinoshima. We also conducted an offline tripartite-array observation. The cross-correlation analysis with five stations supports the results obtained by using the online stations. The typical RMS value is on the order of 0.01 Pa, and the typical duration is several days. The temporal variations of the amplitudes were primarily controlled by the effective sound velocity structure in the atmosphere from Nishinoshima to Chichijima. The infrasonic observations together with the meteorological observation at Chichijima suggest that volcanic eruptions that excite infrasound were not active in the first two weeks in January 2015. This study demonstrates the feasibility of coupling infrasonic observations with meteorological observations for monitoring volcanic eruption at a remote island in nearly real time. Development of the theoretical estimation of the meteorological effects could help us to monitor the eruptive activity more quantitatively.

ACKNOWLEDGMENTS

The authors thank JMA, the JMA Meteorological Observatory at Chichijima, Ogasawara Village Office, Yasushi Ishihara, Kazuto Kawakami, Masashi Kamogawa, and Yuki Suzuki.

REFERENCES

Ben-Menahem, A. & Singh, S. J., 2000. *Seismic Waves and Sources*, Dover Earth Science Series, Dover, 2nd edn.

Che, I. Y., Stump, B. W., & Lee, H. I., 2011. Experimental characterization of seasonal variations in infrasonic traveltimes on the Korean Peninsula with implications for infrasound event location, *Geophysical Journal International*, **185**(1), 190–200.

Drob, D. P. & Picone, J., 2003. Global morphology of infrasound propagation, *Journal of Geophysical Research*, **108**(D21), 4680.

Fee, D. & Matoza, R. S., 2013. An overview of volcano infrasound: From Hawaiian to Plinian, local to global, *Journal of Volcanology and Geothermal Research*, **249**, 123–139.

Fee, D., Steffke, A., & Garces, M., 2010. Characterization of the 2008 Kasatochi and Okmok eruptions using remote infrasound arrays, *Journal of Geophysical Research: Atmospheres*, **115**(18), 1–15.

Fukao, Y., Nishida, K., & Kobayashi, N., 2010. Seafloor topography, ocean infragravity waves, and background Love and Rayleigh waves, *Journal of Geophysical Research*, **115**(B4).

Garcés, M., 2003. Observations of surf infrasound in hawaií, *Geophysical Research Letters*, **30**(24), 3–5.

Haney, M. M., 2009. Infrasonic ambient noise interferometry from correlations of microbaroms, *Geophysical Research Letters*, **36**(19), L19808.

Hedlin, M., Walker, K., Drob, D., & de Groot-Hedlin, C., 2012. Infrasound: Connecting the solid earth, oceans, and atmosphere, *Annual Review of Earth and Planetary Sciences*, **40**(1), 327–354.

Ichihara, M., Takeo, M., Yokoo, A., Oikawa, J., & Ohminato, T., 2012. Monitoring volcanic activity using correlation patterns between infrasound and ground motion, *Geophysical Research Letters*, **39**(February), 1–5.

Kamo, K., Ishihara, K., & Tahira, M., 1994. Infrasonic and seismic detection of explosive eruptions at Sakurajima volcano, Japan, and the PEGASUS-VE early-warning system, *Proc. 1st Int. Symp. Volcanic Ash and Aviation Safety, US Geol. Surv. Bull.*, **2047**, 357–365.

Lacanna, G., Ichihara, M., Iwakuni, M., Takeo, M., Iguchi, M., & Ripepe, M., 2014. Influence of atmospheric structure and topography on infrasonic wave propagation, *Journal of Geophysical Research: Solid Earth*, **119**(4), 2988–3005.

Le Pichon, A., Blanc, E., Drob, D., Lambotte, S., Dessa, J. X., Lardy, M., Bani, P., & Vergniolle, S., 2005. Infrasound monitoring of volcanoes to probe high-altitude winds, *Journal of Geophysical Research*, **110**(D13), D13106.

Nishida, K., Fukao, Y., Watada, S., Kobayashi, N., Tahira, M., Suda, N., Nawa, K., Oi, T., & Kitajima, T., 2005. Array observation of background atmospheric waves in the seismic band from 1 mHz to 0.5 Hz, *Geophysical Journal International*, **162**(3), 824–840.

Ono, Y. & Irino, T., 2004. Southern migration of westerlies in the Northern Hemisphere PEP II transect during the Last Glacial Maximum, *Quaternary International*, **118–119**, 13–22.

Ripepe, M., 2002. Array tracking of infrasonic sources at Stromboli volcano, *Geophysical Research Letters*, **29**(22), 3–6.

Ripepe, M., De Angelis, S., Lacanna, G., & Voight, B., 2010. Observation of infrasonic and gravity waves at Soufrière Hills Volcano, Montserrat, *Geophysical Research Letters*, **37**(8), 1–5.

Ripepe, M., Bonadonna, C., Folch, A., Delle Donne, D., Lacanna, G., Marchetti, E., & Höskuldsson, A., 2013. Ash-plume dynamics and eruption source parameters by infrasound and thermal imagery: The 2010 Eyjafjallajökull eruption, *Earth and Planetary Science Letters*, **366**, 112–121.

Shen, Y., Ren, Y., Gao, H., & Savage, B., 2012. An improved method to extract very-broadband empirical Green's functions from ambient seismic noise, *Bulletin of the Seismological Society of America*, **102**(4), 1872–1877.

Ulivieri, G., Ripepe, M., & Marchetti, E., 2013. Infrasound reveals transition to oscillatory discharge regime during lava fountaining: Implication for early warning, *Geophysical Research Letters*, **40**(12), 3008–3013.

This paper has been produced using the Blackwell Scientific Publications GJI LaTeX2e class file.